Korean J. Chem. Eng., 37(11), 1963-1974 (2020)
DOI: 10.1007/s11814-020-0599-x

pISSN: 0256-1115
eISSN: 1975-7220

Fabrication of antifouling mixed matrix NF membranes by embedding sodium citrate surfactant modified-iron oxide nanoparticles

Abdolreza Moghadassi†, Sara Moradi, and Samaneh Bandehali

Department of Chemical Engineering, Faculty of Engineering, Arak University, Arak 38156-8-8349, Iran
(*Received 27 December 2019 • Revised 27 May 2020 • Accepted 3 June 2020*)

Abstract−PES-based nanofiltration membranes were prepared by phase inversion method. Fe_3O_4 nanoparticles with a constant concentration and sodium citrate in different concentration were incorporated into the PES. The membranes were characterized by Fourier transform infrared spectroscopy (FTIR), Field emission scanning electron microscopy (FESEM), EDX dot mapping and Atomic force microscope (AFM) analysis. Physico-chemical, antifouling properties, and separation performance of the fabricated membranes were investigated by the contact angle, pure water flux (PWF), Na_2SO_4 rejection and flux recovery ratio (FRR%). The membrane porosity and mean pore size enhanced for the modified membranes compared the bare membrane. The PWF sharply improved from 16 L/m^{2}h in the bare membrane to 47 L/m^{2}h at 0.5 wt% Fe_3O_4 and 0.3 wt% sodium citrate (M5). The highest salt rejection obtained was 68%, while it was 61% for the bare membrane. Better dispersion of Fe_3O_4 nanoparticles into the casting solution with outstanding antifouling properties was observed.

Keywords: Nanofiltration Membrane, Iron Oxide Nanoparticle, Sodium Citrate, Antifouling Properties

INTRODUCTION

Nanofiltration membranes as a promising technology have been largely developed in the past decade for different industrial applications, such as water softening, wastewater treatment and other separation and purification techniques. Nanofiltration membranes as pressure-driven membranes contain pores in the range of 0.5-2 nm that can lead to separate different organic molecules with molecular cut off more than 200 Da and multivalent salts [1-3]. Different polymeric materials were used for the preparation NF membranes such as polyethersulfone (PES), polyamides (PAs), polysulfone (PS), polyethylene glycol (PEG). However, polymeric materials with advantages such as low price and easy fabrication process are common materials for NF membrane preparation. But these materials show low thermal stability and low chemical resistance, which limits their applications in NF membranes for a long time [4-8]. Fouling is another phenomenon which reduces the separation performance of NF membranes due to contaminant participation on the membrane surface. There are different methods for overcoming these challenges, such as grafting, coating, additive blending, and surface modification by physical and chemical treatment [9-12]. Among these methods, organic and inorganic nanomaterials such as metal oxides, carbon nanotubes, graphene oxides, silica, zeolites, micro organic frameworks, have been applied as additive materials for the fabrication of high-performance NF polymeric membranes. Metal oxide nanoparticles are widely used as an additive for the optimization of NF membranes. Compared with other metal oxides, iron oxide nanoparticles show significant effects in separation performance of NF membranes, that was confirmed by many studies [13-17].

Fe_3O_4 is a stable iron oxide at ambient conditions. Magnetic oxide nanoparticles show high adsorption capacity, excellent reactivity and high potential to ion exchange. Moreover, they have low cost and environmental safety. But recycling Fe_3O_4 nanoparticles and low dispersity and its aggregation into the membrane matrix or membrane surface are the important challenge [18,19]. Thus, different studies focused on enhancing Fe_3O_4 dispersity and improvement of the recyclability. These studies have applied different methods. For example, the Fe_3O_4 dispersion on the high surface area of a carrier is one solution to improve the dispersion and increase active sites of adsorption. Furthermore, the incorporation of different additives such as ligands enhances the compatibility between polymer and nanoparticles. Moreover, coating nanoparticle by an adsorptive layer and immobilization of a reactive ligand on the nanoparticle surface or combination of these methods are other procedures for the enhancement of Fe_3O_4 properties for application in membrane preparation [20-24].

Alam et al. [25] showed that the incorporation of 10 wt% Fe_3O_4 nanoparticles into the PES as membrane matrix increased the NaCl rejection 68% and $MgSO_4$ rejection 82%, respectively. Ghaemi et al. [13] prepared mixed matrix PES nanofiltration membranes by embedding various concentrations of the modified Fe_3O_4 based nanoparticles. Nanoparticle modification was carried out by immobilizing silica, amine, and metformine. Embedding iron oxide nanoparticles led to a significant increasing of the mean pore radius, porosity and hydrophilicity of the membranes and the pure water flux. Moreover, the copper removal capability of the prepared membranes remarkably increased. In another work, PA6@Fe_xO_y nanofibrous membranes were prepared by electrospinning and hydrothermal method. These nanofibrous membranes exhibited excellent performance for Cr removal from $K_2Cr_2O_7$ solution by using

†To whom correspondence should be addressed.
E-mail: a-moghadassi@araku.ac.ir, A.moghadassi@gmail.com

Freundlich adsorption mechanism [26]. Javaheri and Hassanajili [27] reported the synthesis of Fe_3O_4@SiO_2@MPS@ poly(4-vinylpyridine) nanoparticles that led to high adsorption of nitrate removal. Daraei et al. [28] prepared nanoparticles from Fe_3O_4 coated with polyaniline (PANI). Then the synthesized nanoparticles were applied to coat multi-walled carbon nanotube (MWCNT). These nanoparticles were applied to prepare PES-based mixed matrix membranes. These membranes enhanced anti-fouling properties and membrane hydrophilicity. In another work, polyvinyl pyrrolidone (PVP) was applied as coating Fe_3O_4 that increased the elimination of Congo red dye [29]. Zinadini et al. [30] showed that chemical bonding between carboxymethyl chitosan and Fe_3O_4 on the PES membrane surface improved water flux due to presence of more hydrophilic groups, and the flux recovery ratio (FRR%) obtained was 91.7% for 0.5 wt% nanoparticles.

In this study, sodium citrate was applied as an additive to improve nanoparticle dispersity. Iron oxide nanoparticles are positively charged, but without surfactants tend to be unstable in solution and to aggregate rapidly. There are several classes of surfactants that can be used to form a monolayer on the iron oxide nanoparticle surface, such as sodium citrate [31]. The chemical formula of sodium citrate is $Na_3C_6H_5O_7$. Sodium citrate is a water-soluble surfactant that can be expected to enhance the hydrophilic properties of membrane [32]. Due to the large surface-to-volume ratio, magnetite nanoparticles are highly prone to aggregate in order to reduce their surface energy. Sodium citrate can improve the stability of magnetite nanoparticles due to electrostatic repulsion between nanoparticles. This stability is based on the equilibrium between attractive and repulsive forces [33,34]. Citrate ions have the ability to chelate with the iron molecules, leading to hydrolysis and resulting in particle degradation [35]. Moreover, PES was considered as a polymeric membrane matrix. Because it has excellent film-forming properties, such as high chemical, mechanical stability and good biological resistance [36]. PES is hydrophobic that reduces anti-fouling properties of membranes [36,37]. Therefore, modification of PES membranes was investigated by incorporation of different concentration of iron nanoparticles/sodium citrate surfactant for Na_2SO_4 removal. The separation performance of membranes and membrane antifouling properties was evaluated by pure water flux (PWF), Na_2SO_4 rejection and flux recovery ratio.

EXPERIMENTAL

1. Materials

Polyethersulfone (PES) was purchased from BASF company with M_W=58,000 g/mole as a membrane matrix, polyvinylpyrrolidone (PVP) with M_W=25,000 g/mole was used as pore former, iron oxide (Fe_3O_4) nanoparticles and sodium citrate were supplied from Merck (Germany) as additive, N, N-dimethylacetamide (DMAc) was used as a solvent from Fluka, deionized water was also used as non-solvent (coagulation bath) throughout the experiments. Moreover, the aqueous solutions of sodium sulfate (Na_2SO_4) with M_W=142.04 g/mole were applied from Merck.

2. Membrane Preparation

NF membranes were prepared by phase inversion method. PES as a polymeric matrix with desired concentration, polyvinylpyrrolidone as a pore former, various concentrations of iron oxide nanoparticles and sodium citrate were dissolved in DMAc and stirred by mechanical stirrer at 400 rpm at 8 hours to obtain homogeneous solutions. The prepared solutions were sonicated for 30 min ultrasonically for better dispersion of nanoparticles. The casting solutions were left at ambient temperature for 12 h for air bubble removal. Then, uniform solutions were cast on dry and clean glass plates by an applicator with 150 μm thickness. The cast polymeric films were immediately immersed into deionized water at room temperature (23-25 °C). After 15 minutes, the exchange between solvent and non-solvent was performed. The prepared membranes tacked into the deionized water for 24 hours for the complete phase inversion process. Then, membranes were kept between the two sheets of filter paper. The compositions of the polymeric solutions are shown in Table 1. The chemical structure of used material is shown in Fig. 1.

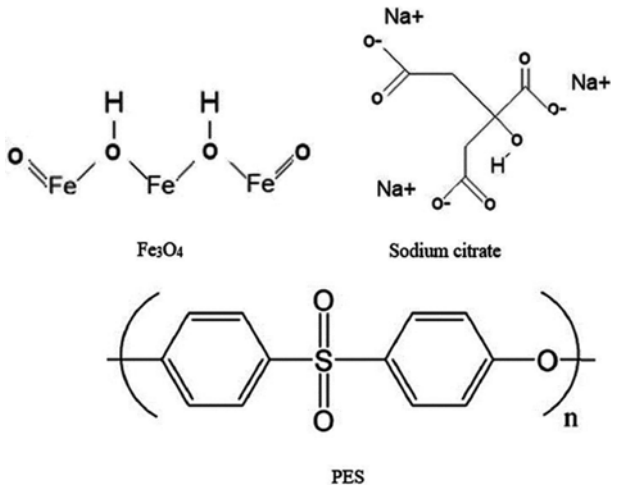

Fig. 1. The chemical structure of used materials in this study.

Table 1. Composition details of casting solutions in membrane preparation

Membranes no.	DMAc (wt%)	PES (wt%)	PVP (wt%)	Fe_3O_4 (wt%)	Sodium citrate (wt%)
M1	81	18	1	0	0
M2	80.5	18	1	0.5	0
M3	80.4	18	1	0.5	0.1
M4	80.3	18	1	0.5	0.2
M5	80.2	18	1	0.5	0.3
M6	80.1	18	1	0.5	0.4
M7	80	18	1	0.5	0.5

3. Characterization Methods

Fourier transform infrared spectroscopy (FTIR) with a Bruker Spectrometer (TENSOR 27) was used to characterize the functional groups of sodium citrate and iron oxide nanoparticles with scanning area 500 to 4,000 cm^{-1} and the resolution of 1 cm^{-1} for each spectrum. Cross-sectional structures of the prepared membranes were monitored and scanned by field emission scanning electron microscopy (FESEM).

Water content was measured by the difference between the dry weight and wet weight of the membranes. The wet weight of membranes was measured by membrane immersion into the deionized water for three days. The wet membranes were dried in an oven at 60 °C for about 4 h. The following equation was used for water content calculation [38-40]:

$$\text{Water content}\,(\%)=\left(\frac{W_w-W_d}{W_w}\right)\times 100 \tag{1}$$

where W_w and W_d are the wet and dry weight (g) of the membranes, respectively. To minimize the experimental errors, all measurements were taken three times and their mean values were reported as the final result.

The water contact angle was used to evaluate the changes in the hydrophobicity and the wetting properties of mixed matrix membranes. Contact angle was measured by the contact angle analyzer and deionized water as a probe liquid. To minimize experimental error, contact angle was measured in five random locations for each sample and then their average was reported.

The following equation was used for the calculation of the overall porosity (ε):

$$\varepsilon(\%)=\left(\frac{W_w-W_d}{\rho_f V_m}\right)\times 100 \tag{2}$$

where W_w, W_d, ρ_f and V_m are the wet and dry weight (g) of the membranes, water density (g/cm^3) and membrane volume (cm^3), respectively. Three experiments were performed on each sample to reduce experimental error and then the mean values were reported.

The filtration velocity method using the Guerout-Elford-Ferry equation was used to estimate the mean pore size of the modified membranes [41]:

$$r_m=\sqrt{\frac{(2.9-1.75\varepsilon)8\eta LQ}{\varepsilon A\Delta p}} \tag{3}$$

where η, L and Q are the water viscosity (8.9×10^{-4} Pa·s), the membrane thickness (m) and the volume of the permeated pure water flux (m^3/s), ε is membrane porosity, A is the membrane filtration area (m^2) and Δp is operating pressure (0.45 MPa).

4. Membrane Separation Performance Test

The pure water flux (PWF) and salt rejection were measured using a stirred dead-end cell filtration system with an effective surface area of 11.94 cm^2. Before using and analyzing the samples, the membranes were first compressed with deionized water at 0.5 MPa for 15 minutes. Then, the operating pressure for filtration experiments was changed to 0.45 MPa. The PWF was measured and was defined as $j_{w,1}$ (L/m^2h). In addition, an aqueous solution of Na_2SO_4 (0.01 mol/L) as feed solution was used to evaluate the performance of NF membranes.

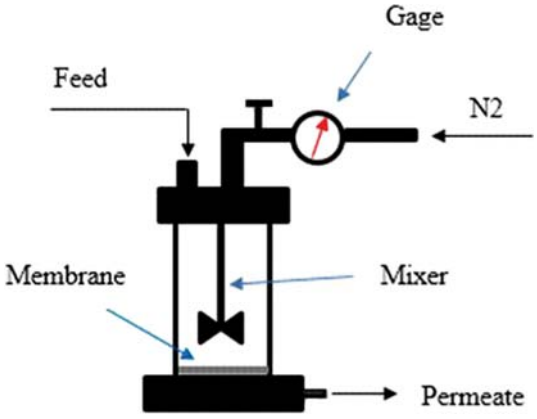

Fig. 2. The dead-end filtration setup for evaluation of membrane performance [42].

The following equations were used for the calculation of PWF and rejection:

$$j_{w,1}=\left(\frac{V}{A\Delta t}\right) \tag{4}$$

$$R(\%)=\left(\frac{C_f-C_p}{C_f}\right)\times 100 \tag{5}$$

where V, A, Δt, C_f and C_p are volume of permeate flux (m^3), membrane area (m^2), sampling time (h), ions concentration in feed and permeate, respectively. Fig. 2 shows the dead-end filtration setup for evaluation of membrane performance.

Subsequently, the permeate flux of BSA aqueous (J_P, L/m^2h) with a concentration of 8,000 mg/L was used as a damaging agent in the range of 0.45 MPa for 2 hours based on the amount of transferred water from the membrane to determine the flux recovery ratio. Fouled membranes were washed with distilled water for 15 minutes after filtering the milk solution and the PWF $J_{w,2}$ (L/m^2h), was remeasured and flux recovery ratio (FRR%) was calculated as the following equation:

$$FRR(\%)=\left(\frac{J_{w,2}}{J_{w,1}}\right)\times 100 \tag{6}$$

RESULTS AND DISCUSSION

1. Characterization of Sodium Citrate-iron Oxide Nanoparticles

The FTIR analysis of iron oxide nanoparticles and sodium citrate is shown in Fig. 3 (sodium citrate (a), iron oxide nanoparticles (b), and prepared membranes (c)). As shown in Fig. 3(a) the specific bands at 1,421 cm^{-1} and 1,588 cm^{-1} are related to the symmetric and antisymmetric stretching of the -COO^- groups, and the peak at 3,252 cm^{-1} is due to the tensile vibration of -OH groups in sodium citrate [43]. The FTIR spectra of pure Fe_3O_4 nanoparticles were analyzed in the range of 400-4,000 cm^{-1} and are shown in Fig. 3(b). The FTIR spectrum of Fe_3O_4 shows the broad and the strong absorption peak at 574 cm^{-1} that reveals the presence of a Fe-O bond of Fe_3O_4 nanoparticles. A broad peak at 3,431 cm^{-1} represents the O-H stretching groups [44]. Fig. 3(c) shows the FTIR spectrum of the iron oxide/sodium citrate containing PES mem-

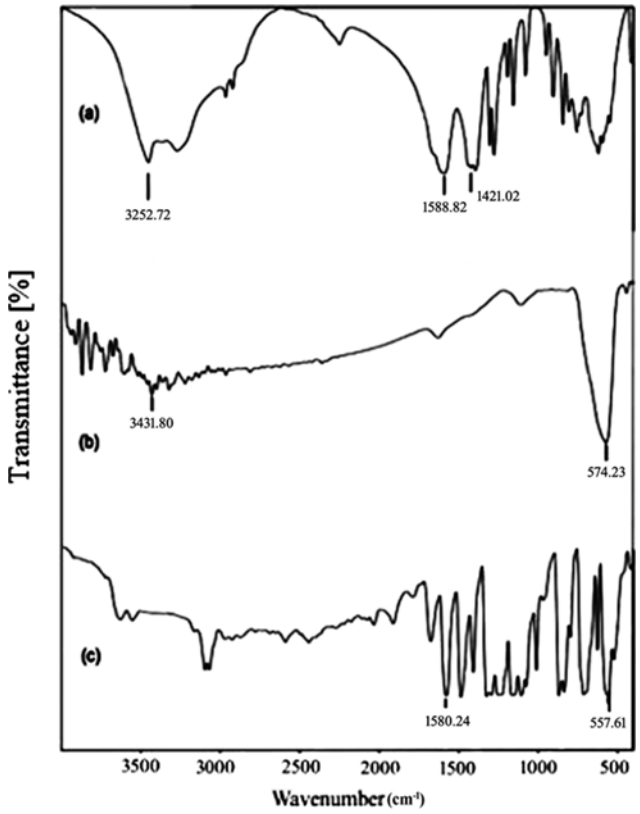

Fig. 3. FTIR spectra of (a) sodium citrate, (b) iron oxide and (c) iron oxide/sodium citrate containing PES membranes.

branes. As is clear in Fig. 3(c), the peaks at 1,580 and 557 cm^{-1} are due to -COO^- and Fe-O bonds, respectively. Moreover, the peak in the range of 1,258.72 to 1,275.84 cm^{-1} is attributed to the presence of C=SO_2=C. Also, the peak in the range of 1,479.82-1,599.30 cm^{-1} is due to benzene ring stretching in the PES membrane [45].

2. Membrane Characterization

2-1. Membrane Morphology

The cross-sectional FESEM images were used to study the changes of morphology and dispersion of iron oxide nanoparticles (0.5 wt%) at different concentrations of sodium citrate surfactant. As is clear in the FESEM images (Fig. 4), all samples have an asymmetric structure with a dense upper layer and a porous sub-layer. The addition of hydrophilic nanoparticles to a polymer solution affects the exchange rate between non-solvent and solvent [46]. Faster solvent removal results in the rapid formation of the active layer, which creates an excess resistance to the mass transfer and increases the required time for the solvent and non-solvent exchange in sublayer; therefore, the cavities in the sublayer from the sponge-like structure convert to a finger-like structure [47-49]. FESEM images showed that increasing sodium citrate in the membrane structure resulted in a significant increase of the size of finger-like channels in the sub-layer of the modified membranes compared with the neat PES membrane [50]. The presence of sodium citrate as an anionic and hydrophilic additive with similar properties of non-solvent (water) in a polymeric solution leads to greater polymer insolubility due to the formation of sodium citrate-polymer bonds, which reduces the interaction of polymer chains. This eventually leads to a faster phase inversion of the polymer solution in non-solvent. As a result, this kind of behavior leads to the formation of larger cavities in the membrane structure [46,51]. Thus, due to the hydrophilicity of sodium citrate and the iron oxide nanoparticles, the phase inversion occurred faster, the membrane cavities formed the finger-like structure and water flux increased. Moreover, the FESEM images of membranes surface (Fig. 5) confirmed the good dispersion of Fe_3O_4 nanoparticles by the incorporation of sodium citrate. The cross sectional mapping analysis of Fe element is shown in Fig. 6 for M2 (at 0.5 wt% iron oxide nanoparticles) and M3 (at 0.5 wt% of iron oxide nanoparticles and 0.1 wt% sodium citrate). As shown in this figure, the dispersion of Fe element in membrane containing of sodium citrate is better than

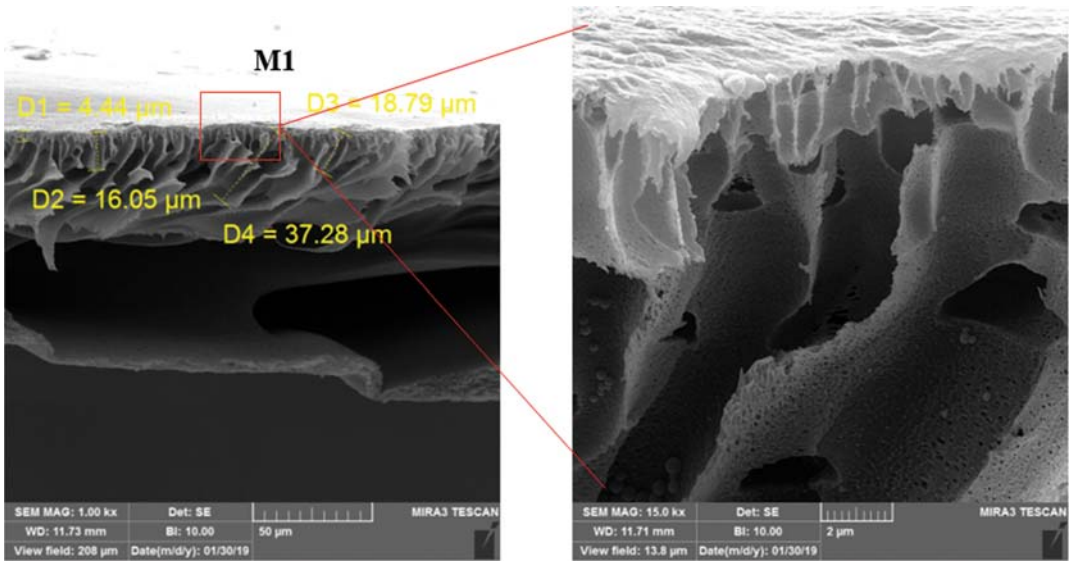

Fig. 4. The FESEM cross sectional images of the prepared membranes with 0.5 wt% iron oxide and different concentrations of sodium citrate.

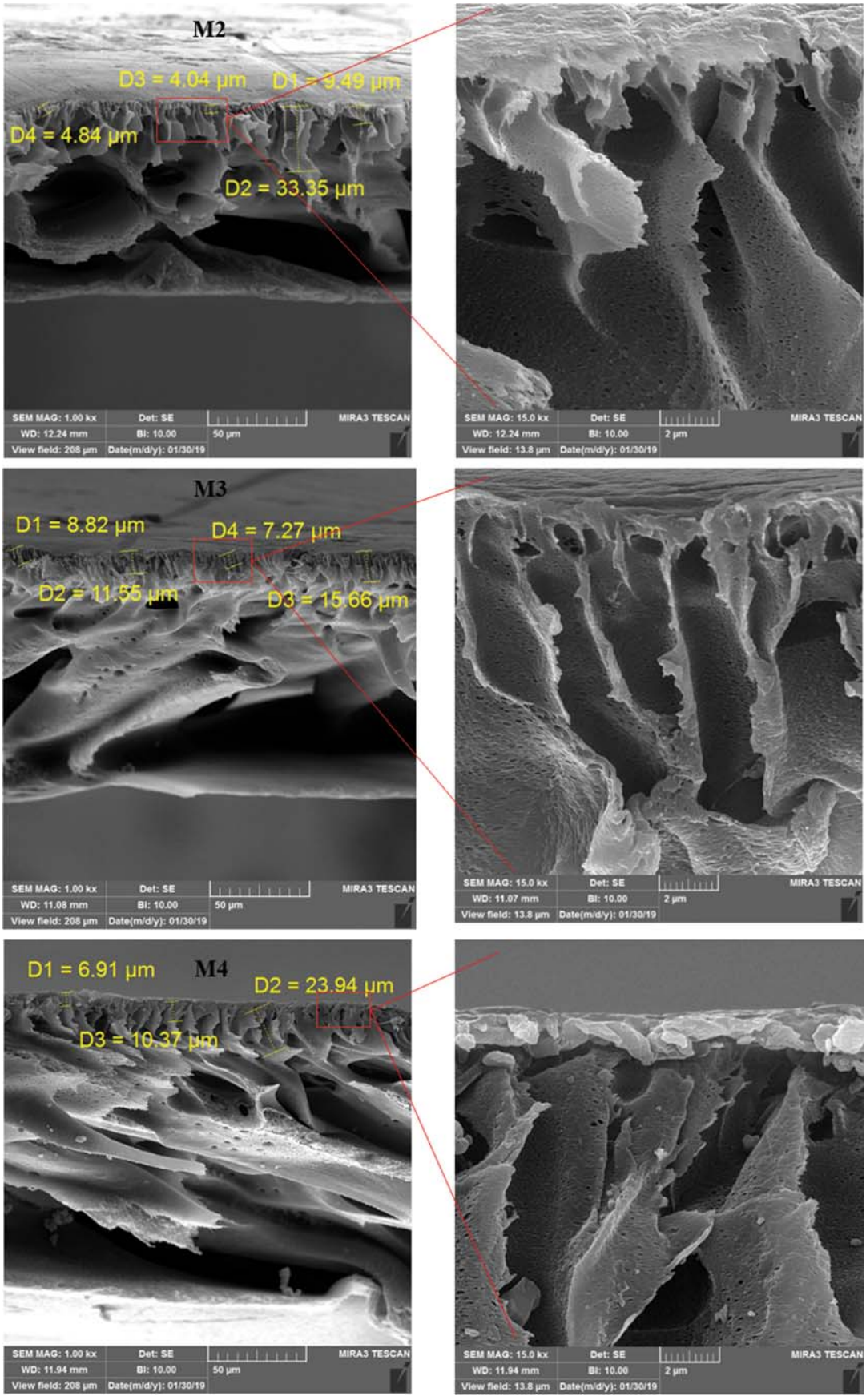

Fig. 4. Continued.

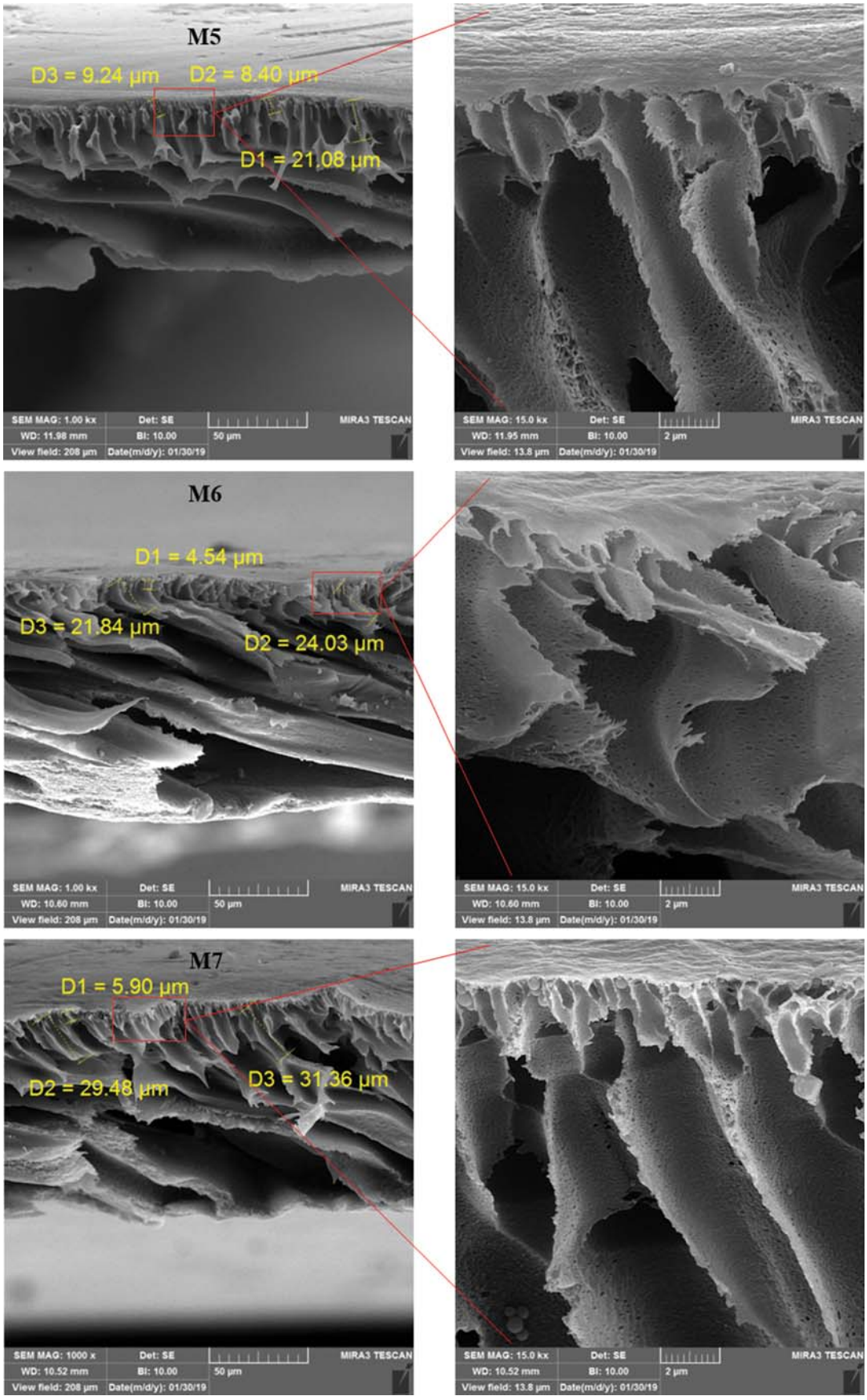

Fig. 4. Continued.

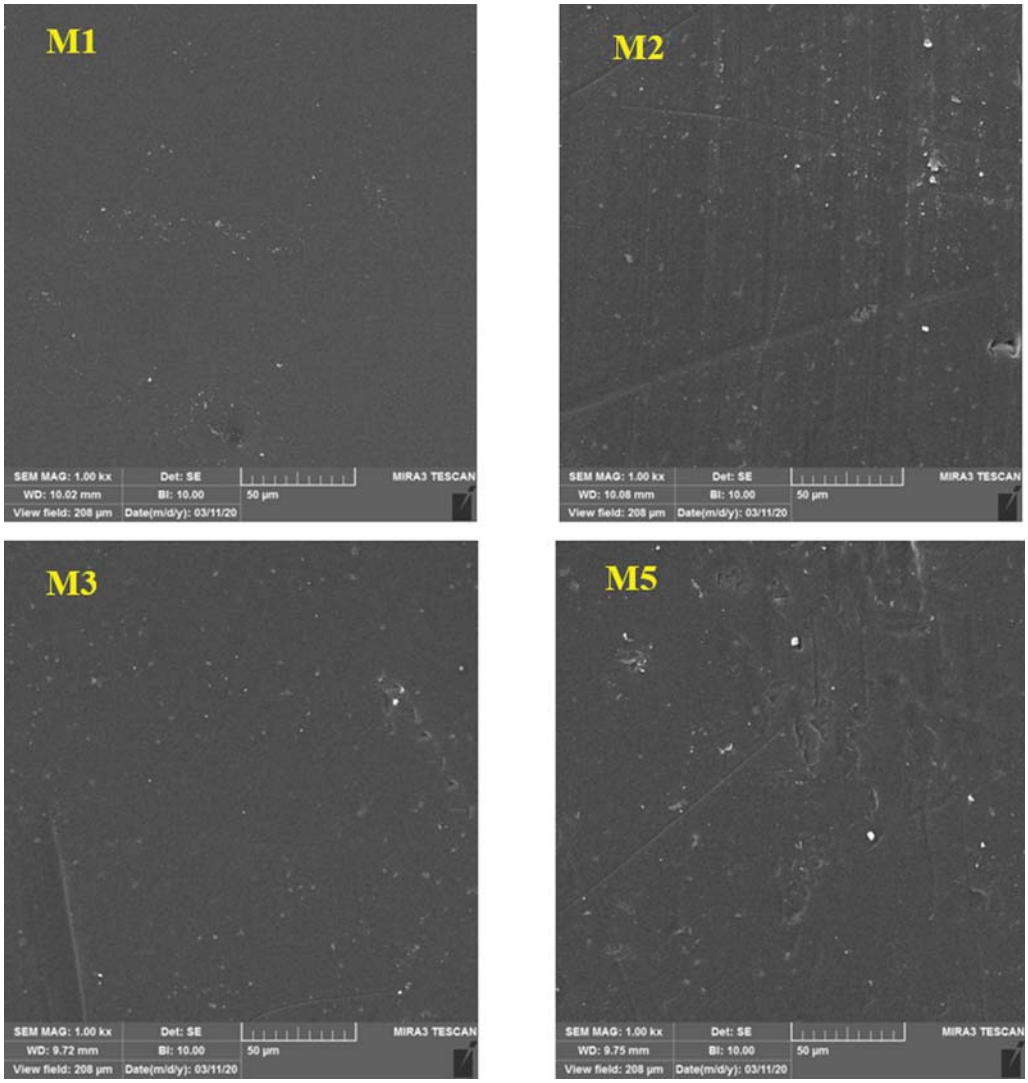

Fig. 5. The FESEM surface images of the prepared membranes (M1, M2, M3 and M5).

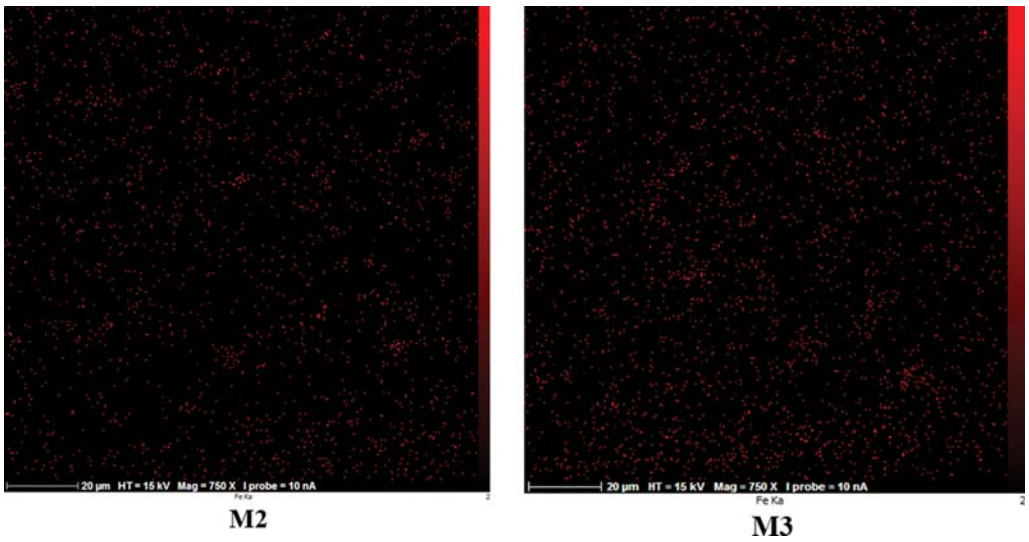

Fig. 6. EDX dot mapping distribution of Fe element for M2 (at 0.5 wt% iron oxide nanoparticles) and M3 (at 0.5 wt% of iron oxide nanoparticles and 0.1 wt% sodium citrate).

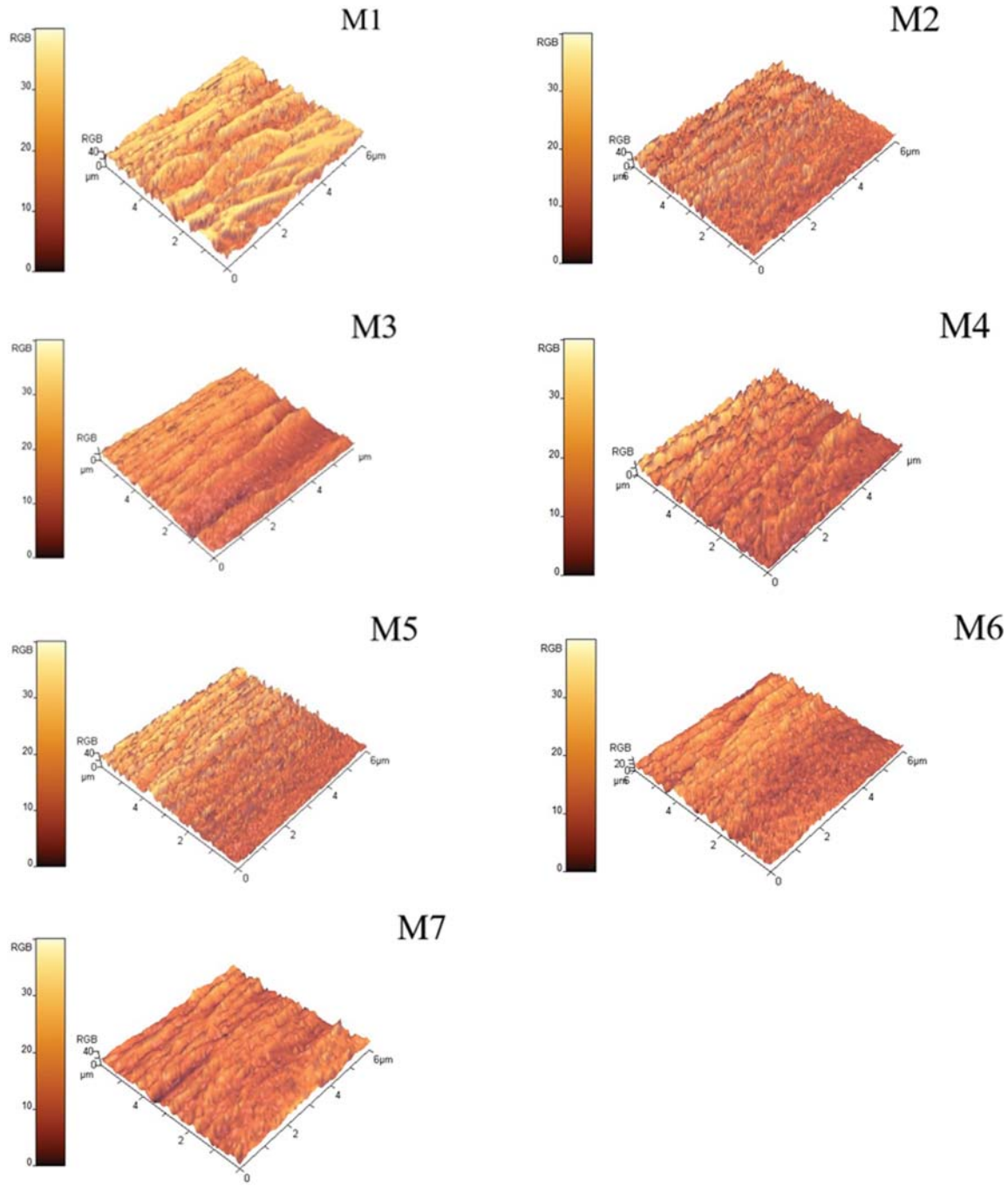

Fig. 7. AFM images of the prepared membranes at 0.5 wt% iron oxide and different concentrations of sodium citrate.

membranes containing of only iron oxide nanoparticles.

For the investigation of surface morphology, atomic force microscopy (AFM) was used and roughness parameters such as mean roughness (R_a) and root mean square (R_q) of membranes were measured. Fig. 7 shows three-dimensional images of the membrane surface. The high roughness of the membrane surface can be due to increasing the pore size [52]. As one can see in Table 2, the membranes M3, M6 and M7 have less R_a, also have smaller cavities in the active layer according to cross-sectional images of the membranes in the FESEM images. The incorporation of nanoparticles

Table 2. The roughness parameter of the prepared membranes

Membrane No.	R_a (nm)	R_q (nm)
M1	7.5	8.6
M2	6.0	7.5
M3	4.6	5.5
M4	6.2	7.9
M5	5.8	7.3
M6	5.1	6.2
M7	4.8	5.6

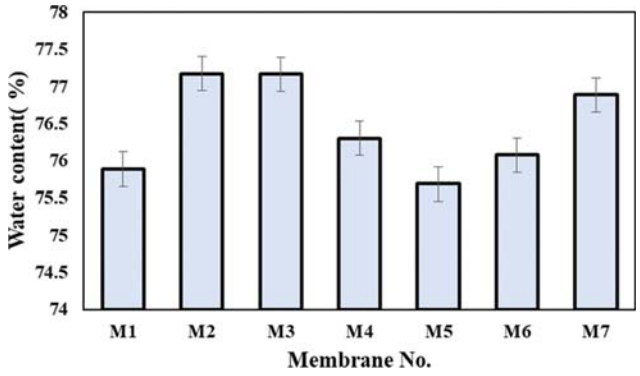

Fig. 8. Water content measurements for the prepared membranes.

into the membrane decreased surface roughness compared with the neat PES membrane [13,53]. Because of the hydrophilicity of sodium citrate and iron oxide nanoparticles, phase inversion occurred faster, and hydrophilic nanoparticles transferred to the surface of the membrane; thus the surface of the membrane became more hydrophilic and decreased roughness [47].

3. Membrane Filtration Performance

3-1. Water Content and Contact Angle

Contact angle and water content studies were used to evaluate the effect of iron nanoparticles and sodium citrate surfactant on the hydrophilicity and wetting of the prepared membranes. According to the obtained values, the water content of the modified membranes increased compared to the neat PES membrane. Because, iron oxide as a hydrophilic nanoparticle and sodium citrate as a water-insoluble surfactant increase the hydrophilicity of membranes [32]. Fig. 8 shows that the membrane water content initially increased with increasing iron oxide nanoparticles, which can be due to the hydrogen bonding between iron oxide nanoparticles and water molecules, and then it reduced by increasing sodium citrate due to improvement in the rate of phase inversion process and the formation of larger and longer pores. Therefore, the membrane ability was reduced to water retention. While water content was enhanced in a high concentration of sodium citrate (M7), that can be due to solubility of sodium citrate in water and thus reduction of water transport from membrane pores.

The water contact angle of the prepared membranes was measured to evaluate the hydrophilicity changes after adding iron oxide nanoparticles and sodium citrate to the membrane structure. The results showed that all iron oxide nanoparticles and sodium citrate containing membranes have a lower contact angle than the neat PES membrane which is attributed to increasing hydrophilic groups in the membrane. Note that iron oxide nanoparticles with hydroxyl groups come to the membrane surface due to their hydrophilicity during the phase inversion process, and the presence of hydrophilic nanoparticles on the membrane surface leads to higher hydrophilicity of the membrane surface [18,54]. The water contact angles are presented in Table 3.

3-2. Pure Water Flux and Salt Rejection

Pure water flux (PWF) was determined for membranes with different concentrations of sodium citrate surfactant and 0.5 wt% of Fe_3O_4. The results are presented in Fig. 9. PWF of prepared membranes increased with increasing sodium citrate concentrations compared with neat PES membranes (16 L/m^{2}h). The maximum PWF (47 L/m^{2}h) was observed in M5 membrane for 0.3 wt% sodium citrate. Decreasing PWF for M2 can be explained due to the aggregations of iron nanoparticles and bad dispersion of nanoparticles in the membrane structure, but in subsequent membranes the dispersity of nanoparticles improved due to the increase of sodium citrate surfactant. The membrane filtration performance is directly related to the hydrophilicity and membrane structure. Increasing the hydrophilicity of the membrane surface leads to more water absorption and increasing the energy of interaction between the surface of the membrane and the water molecules, so that their results is the enhancement of wettability and pure water flux [41, 55]. Use of nanoparticles and sodium citrate surfactant increased

Table 3. Water contact angle measurements for the prepared membranes

Membrane No.	Contact angle (°)
M1	60.2
M2	55.5
M3	41.1
M4	58.7
M5	51.3
M6	39.8
M7	48.8

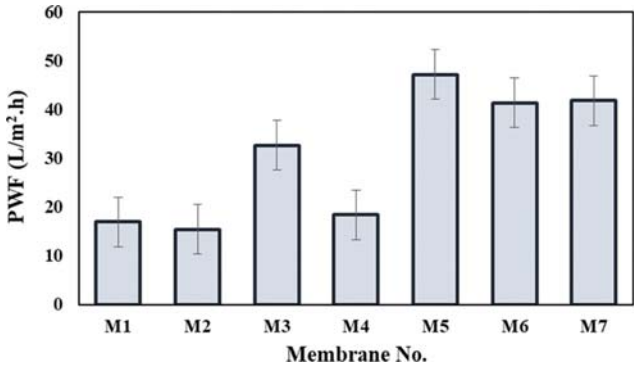

Fig. 9. Pure water flux of the prepared membranes.

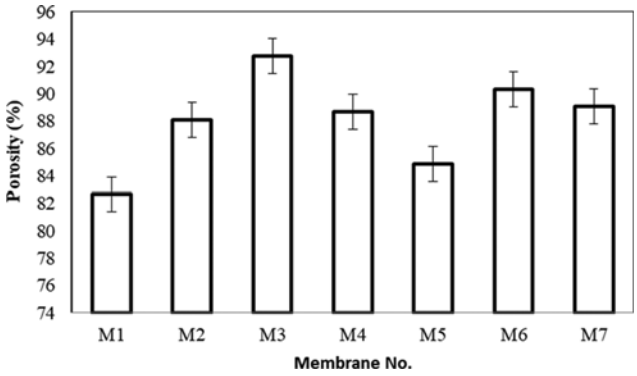

Fig. 10. Overall porosity of the prepared membranes.

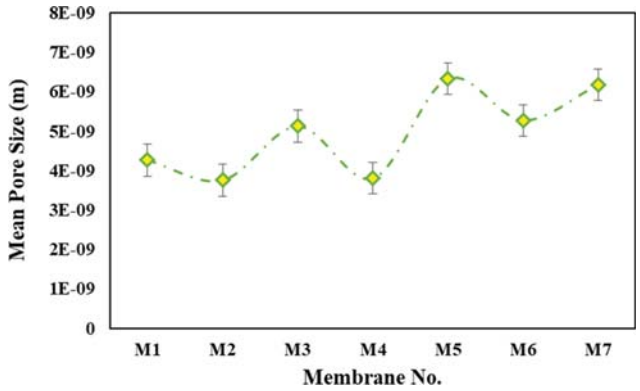

Fig. 11. Calculated mean pore size of the prepared membranes.

the hydrophilicity and water content. Moreover, increasing sodium citrate, increases porosity of the prepared membranes compared to the neat PES membrane (see Fig. 10), that is according to FESEM images. Moreover, the mean pore size of prepared membranes increases (see Fig. 11). But nanoparticle agglomeration on the surface and inside the membrane can play an important role in the size of cavities in the membrane structure. In these conditions, the transport channels can be blocked and thus reduce the flux [41, 56,57]. The highest mean pore size observed for M5 led to increase PWF to 47 L/m^{2}h.

Due to the interaction among the membrane, nanoparticles and sodium citrate, the membrane surface charge could be an effective feature that affects the membrane performance due to negative charges of nanoparticles and sodium citrate [58]. Iron oxide contains hydroxyl groups with negative charges that lead to electrostatic repulsion SO_4^{-2} ions. This mechanism is the major reasons for Na_2SO_4 separation. Moreover, increasing the negative charges of the membrane surface enhances by adding sodium citrate because sodium citrate has hydroxyl group too that led to electrostatic repulsion SO_4^{-2} ions [46]. Fig. 12 shows the Na_2SO_4 rejection and the flux by membranes. All prepared membranes show higher rejection than the neat PES membrane, and this is due to present negative charges. The Na_2SO_4 rejection increased with increasing

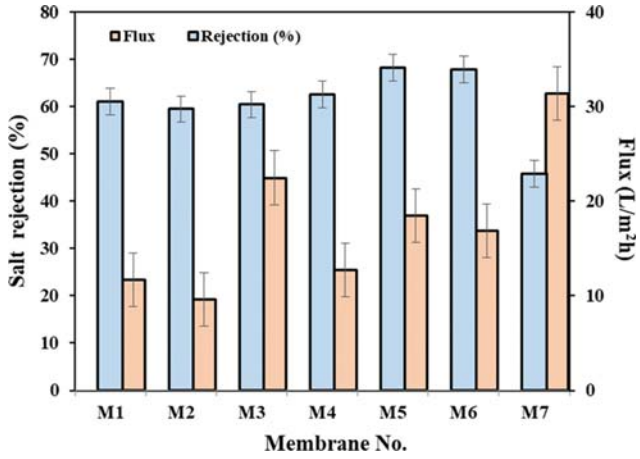

Fig. 12. Rejection and flux of the prepared membranes for Na_2SO_4 separation.

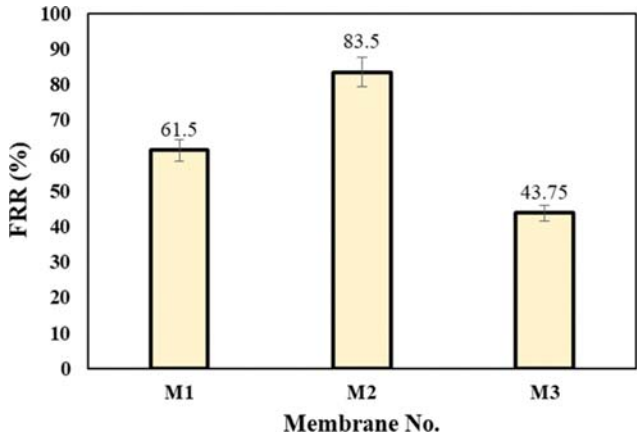

Fig. 13. Flux recovery ratio of the prepared membranes.

nanoparticle concentration and the highest Na_2SO_4 rejection was obtained for M5 and M6. Moreover, the increase of sodium citrate enhanced the iron oxide dispersion in the membrane structure that led to more effectiveness of functional groups in modified membranes. Therefore, Donnan exclusion effects are the main mechanisms for Na_2SO_4 removal. Furthermore, molecular size of ion salts affects the salt ion rejection due to filling surface pores by nanoparticles and the formation of denser layer on the membrane surface [59,60]. M2 has a slight increase in the rejection due to the aggregations of nanoparticles and bad dispersion of nanoparticles. M3 showed a good flux, while its rejection did not have a significant change compared with neat PES membrane.

According to the obtained information by the roughness of the membrane surface, it is observed that M1, M2 and M4 membranes have more roughness and have a higher active surface. But the flux decreased due to the hydrophobicity of the M1 membrane and possibly the fouling in the M2 and M4 membranes. In addition, the flux in all modified membranes was larger than the neat PES membrane, except for the M2 membrane, due to bad dispersion of iron oxide nanoparticles and probably blockages of cavities in a high concentration of nanoparticles [55].

3-3. Antifouling Properties

Membrane hydrophilicity is the most important reason for reducing fouling. The anti-fouling properties of the prepared membranes can be evaluated by flux recover ratio (FRR%) [61]. As shown in Fig. 13, the best anti-fouling properties were obtained for M2. The presence of hydrophilic nanoparticles improved hydrophilicity and anti-fouling properties of prepared membranes. Improvement of the membrane structure and surface properties can reduce the membrane fouling. The enhancement of antifouling properties of membranes leads to energy saving and lower costs [62,63].

CONCLUSION

PES-based nanofiltration membranes were fabricated in the incorporation of Fe_3O_4 and sodium citrate into the PES. The incorporation of sodium citrate improved the dispersion of iron oxide nanoparticles into the membrane structure. The presence of hydrophilic groups enhanced PWF significantly. A smoother surface was

obtained by the incorporation of sodium citrate and iron oxide nanoparticles compared with the neat PES membrane. The highest PWF (47 L/m^{2}h) and Na_2SO_4 rejection (68%) was observed for M5. The PWF enhanced due to increase porosity and mean pore size of membranes and the present more hydrophilic groups. Moreover, the increasing rejection can be attributed to creating more active sites for adsorption of Na_2SO_4 and the presence of negative charges and SO_4^{2-} repulsion. Furthermore, good dispersion of Fe_3O_4 nanoparticles and high hydrophilic properties of membrane surface enhanced antifouling properties of the fabricated membranes.

REFERENCES

1. R. Hu, R. Zhang, Y. He, G. Zhao and H. Zhu, *J. Membr. Sci.*, **564**, 813 (2018).
2. S. S. Madaeni, N. Arast, F. Rahimpour and Y. Arast, *Desalination*, **280**, 305 (2011).
3. Y. Ji, W. Qian, Y. Yu, Q. An, L. Liu, Y. Zhou and C. Gao, *Chin. J. Chem. Eng.*, **25**, 1639 (2017).
4. M. Mertens, T. Van Dyck, C. Van Goethem, A. Y. Gebreyohannes and I. F. Vankelecom, *J. Membr. Sci.*, **557**, 24 (2018).
5. S. Bandehali, A. Moghadassi, F. Parvizian and S. Hosseini, *Korean J. Chem. Eng.*, **36**, 1657 (2019).
6. M. Maarefian, S. Bandehali, S. Azami, H. Sanaeepur and A. Moghadassi, *Int. J. Energy Chem.*, **43**, 8217 (2019).
7. S. Bandehali, F. Parvizian, A. R. Moghadassi, S. M. Hosseini and J. N. Shen, *J. Polym. Res.*, **27**, 94 (2020).
8. S. M. Hosseini, F. Karami, S. K. Farahani, S. Bandehali, J. Shen, E. Bagheripour and A. Seidypoor, *Korean J. Chem. Eng.*, **37**, 866 (2020).
9. S. Zinadini, A. A. Zinatizadeh, M. Rahimi, V. Vatanpour, H. Zangeneh and M. Beygzadeh, *Desalination*, **349**, 145 (2014).
10. S. Bandehali, F. Parvizian, A. Moghadassi and S. M. Hosseini, *Sep. Purif. Technol.*, **237**, 116361 (2019).
11. H. Sanaeepur, A. Ebadi Amooghin and S. Bandehali, *Theoretical gas permeation models for mixed matrix membranes*, LAP LAMBERT Academic Publishing, Beau Bassin, Mauritius (2018).
12. H. Sanaeepur, A. E. Amooghin, S. Bandehali, A. Moghadassi, T. Matsuura and B. Van der Bruggen, *Prog. Polym. Sci.*, **91**, 80 (2019).
13. N. Ghaemi, S. S. Madaeni, P. Daraei, H. Rajabi, S. Zinadini, A. Alizadeh, R. Heydari, M. Beygzadeh and S. Ghouzivand, *Chem. Eng. J.*, **263**, 101 (2015).
14. S. Bandehali, A. Kargari, A. Moghadassi, H. Saneepur and D. Ghanbari, *Asia-Pac J. Chem. Eng.*, **9**, 638 (2014).
15. S. Bandehali, A. Moghadassi, F. Parvizian, S. M. Hosseini, T. Matsuura and E. Joudaki, *J. Energy Chem.*, **46**, 30 (2020).
16. S. Bandehali, F. Parvizian, A. R. Moghadassi and S. M. Hosseini, *J. Polym. Res.*, **26**, 211 (2019).
17. S. Bandehali, H. Sanaeepur, A. Ebadi Amooghin and A. Moghadassi, *Modeling in membranes and membrane-based processes*, A. Roy, S. Moulik, R. Kamesh, A. Mullick Eds., John Wiley & Sons publications, New Jersey (2020).
18. P. Daraei, S. S. Madaeni, N. Ghaemi, E. Salehi, M. A. Khadivi, R. Moradian and B. Astinchap, *J. Membr. Sci.*, **415**, 250 (2012).
19. N. A. Weerasekara, K.-H. Choo and S.-J. Choi, *J. Membr. Sci.*, **447**, 87 (2013).
20. H. Zangeneh, A. A. Zinatizadeh, S. Zinadini, M. Feyzi and D. W. Bahnemann, *React. Funct. Polym.*, **127**, 139 (2018).
21. N. Abdali, A. Marjani, F. Heidary and M. Adimi, *New J. Chem.*, **41**, 6405 (2017).
22. A. Gholami, A. Moghadassi, S. Hosseini, S. Shabani and F. Gholami, *J. Ind. Eng. Chem.*, **20**, 1517 (2014).
23. A. R. Moghadassi, E. Bagheripour and S. M. Hosseini, *J. Appl. Polym. Sci.*, **134**, 44993 (2017).
24. S. M. Hosseini, M. Afshari, A. R. Fazlali, S. Koudzari Farahani, S. Bandehali, B. Van der Bruggen and E. Bagheripour, *Chem. Eng. Res. Des.*, **147**, 390 (2019).
25. J. Alam, L. A. Dass, M. Ghasemi and M. Alhoshan, *Polym. Compos.*, **34**, 1870 (2013).
26. C.-J. Li, Y.-J. Li, J.-N. Wang and J. Cheng, *Chem. Eng. J.*, **220**, 294 (2013).
27. F. Javaheri and S. Hassanajili, *J. Appl. Polym. Sci.*, **133**, 44330 (2016).
28. P. Daraei, S. S. Madaeni, N. Ghaemi, M. A. Khadivi, B. Astinchap and R. Moradian, *Sep. Purif. Technol.*, **109**, 111 (2013).
29. G. Pandey, S. Singh and G. Hitkari, *Int. Nano Lett.*, **8**, 111 (2018).
30. S. Zinadini, A. Zinatizadeh, M. Rahimi, V. Vatanpour, H. Zangeneh and M. Beygzadeh, *Desalination*, **349**, 145 (2014).
31. P. I. Soares, A. M. Alves, L. C. Pereira, J. T. Coutinho, I. M. Ferreira, C. M. Novo and J. P. Borges, *J. Colloid Interface Sci.*, **419**, 46 (2014).
32. K. Kimura, G. Amy, J. Drewes and Y. J. J. o. M. S. Watanabe, *J. Membr. Sci.*, **221**, 81 (2003).
33. H. Mohammad-Beigi, S. Yaghmaei, R. Roostaazad, H. Bardania and A. Arpanaei, *Physica E.*, **44**, 618 (2011).
34. M. Morales, O. Bomati-Miguel, R. P. De Alejo, J. Ruiz-Cabello, S. Veintemillas-Verdaguer and K. O'Grady, *J. Magn. Magn. Mater.*, **266**, 102 (2003).
35. C. Hoskins, A. Cuschieri and L. Wang, *J. Nanobiotechnol.*, **10**, 15 (2012).
36. Q. Shi, Y. Su, S. Zhu, C. Li, Y. Zhao and Z. Jiang, *J. Membr. Sci.*, **303**, 204 (2007).
37. P. D. Peeva, T. Pieper and M. Ulbricht, *J. Membr. Sci.*, **362**, 560 (2010).
38. J. Khan, B. P. Tripathi, A. Saxena and V. K. Shahi, *Electrochim. Acta*, **52**, 6719 (2007).
39. G.-J. Hwang, H. Ohya and T. Nagai, *J. Membr. Sci.*, **156**, 61 (1999).
40. S.-H. Chen, R.-M. Liou, C.-L. Lai, M.-Y. Hung, M.-H. Tsai and S.-L. Huang, *Desalination*, **234**, 221 (2008).
41. E. Bagheripour, A. R. Moghadassi, S. M. Hosseini, B. Van der Bruggen and F. Parvizian, *J. Ind. Eng. Chem.*, **62**, 311 (2018).
42. E. Bagheripour, A. R. Moghadassi and S. M. Hosseini, *Arab. J. Chem.*, **10**, S3375 (2017).
43. A. Giri, A. Makhal, B. Ghosh, A. Raychaudhuri and S. Pal, *Nanoscale*, **2**, 2704 (2010).
44. S. R. Kumar, L. Marianna, S. Gianni, A. J. Nathanael, S. Hong, T. H. Oh, D. Mangalaraj, C. Viswanathan and N. Ponpandian, *Mater. Res. Express*, **1**, 015015 (2014).
45. H. Abdul Mannan, H. Mukhtar, M. Shima Shaharun, M. Roslee Othman and T. Murugesan, *J. Appl. Polym. Sci.*, **133**, 1 (2016).
46. N. Ghaemi, S. S. Madaeni, A. Alizadeh, P. Daraei, V. Vatanpour and M. Falsafi, *Desalination*, **290**, 99 (2012).
47. Y. Mansourpanah, S. Madaeni, A. Rahimpour, M. Adeli, M. Hashemi and M. Moradian, *Desalination*, **277**, 171 (2011).
48. F. Parvizian, F. Ansari and S. Bandehali, *Chem. Eng. Res. Des.*, **156**, 433 (2020).

49. S. Bandehali, A. Moghadassi, F. Parvizian, Y. Zhang, S. M. Hosseini and J. Shen, *Sep. Purif. Technol.*, **242**, 116745 (2020).
50. N. Ghaemi, S. S. Madaeni, A. Alizadeh, P. Daraei, A. A. Zinatizadeh and F. Rahimpour, *Sep. Purif. Technol.*, **85**, 147 (2012).
51. E. Bagheripour, A. Moghadassi and S. M. Hosseini, *Asia-Pac J. Chem. Eng.*, **10**, 791 (2015).
52. N. Ghaemi, S. S. Madaeni, A. Alizadeh, H. Rajabi and P. Daraei, *J. Membr. Sci.*, **382**, 135 (2011).
53. M. Peyravi, M. Jahanshahi, A. Rahimpour, A. Javadi and S. Hajavi, *Chem. Eng. J.*, **241**, 155 (2014).
54. A. J. J. F. Kingma and B. Processing, *Food Bioprod. Process.*, **93**, 304 (2015).
55. G. Lai, W. Lau, P. Goh, A. Ismail, N. Yusof and Y. Tan, *Desalination*, **387**, 14 (2016).
56. E. Bagheripour, A. Moghadassi and S. M. Hosseini, *Korean J. Chem. Eng.*, **33**, 1462 (2016).
57. H. M. Hegab and L. Zou, *J. Membr. Sci.*, **484**, 95 (2015).
58. Y. Zhao and Q. Yuan, *J. Membr. Sci.*, **279**, 453 (2006).
59. R. W. Baker, *Membrane technology and applications*, 3th Ed., John Wiley and Sons, West Sussex, UK (2012).
60. S. Bandehali, A. Moghadassi, F. Parvizian, J. Shen and S. Hosseini, *Korean J. Chem. Eng.*, **37**, 263 (2020).
61. M. Amirilargani, M. Sadrzadeh, E. Sudhölter and L. de Smet, *Chem. Eng. J.*, **289**, 562 (2016).
62. S. Madaeni, S. Zinadini and V. Vatanpour, *Sep. Purif. Technol.*, **111**, 98 (2013).
63. Y. Mansourpanah, A. Rahimpour, M. Tabatabaei and L. Bennett, *Desalination*, **419**, 79 (2017).